Magnetic Resonance Letters 3 (2023) 248–255

Contents lists available at ScienceDirect

Magnetic Resonance Letters

journal homepage: www.keaipublishing.com/MRL

Mini Research

Functional group resolved NMR relaxation of 3-carbon adsorbates in mesoporous alumina

Neil Robinson [a,*], Carmine D'Agostino [b,c], Michael L. Johns [a]

[a] Department of Chemical Engineering, The University of Western Australia, 35 Stirling Highway, Perth, WA 6009, Australia
[b] Department of Chemical Engineering, The University of Manchester, Oxford Road, Manchester, M13 9PL, UK
[c] Dipartimento di Ingegneria Civile, Chimica, Ambientale e Dei Materiali (DICAM), Alma Mater Studiorum — Università di Bologna, Via Terracini, 28, Bologna, 40131, Italy

ARTICLE INFO

Article history:
Received 15 January 2023
Received in revised form 13 April 2023
Accepted 8 May 2023
Available online 24 May 2023

Keywords:
NMR relaxation
Adsorption
Porous media
Low-field NMR

ABSTRACT

NMR relaxation analysis provides a unique and non-invasive probe of fluid dynamics within porous materials, and may be applied to the interpretation of a wide variety of material and interfacial characteristics. Here, we report two-dimensional ^{1}H T_1–T_2 relaxation correlation measurements of a range of three-carbon adsorbates (1-propanol, 2-propanol and propanoic acid) imbibed within the mesoporous metal oxide gamma-alumina. Our data, acquired across field strengths of 2 MHz, 12.7 MHz and 43 MHz, clearly reveal two populations in each measurement, identified as the alkyl and hydroxyl moieties of each adsorbate. These results expand the range of materials in which such functional group resolved relaxation is known to occur, and demonstrate the clear persistence of such phenomena using a range of typical benchtop NMR systems employed to study fluid-saturated porous media.

1. Introduction

Measurement of the longitudinal (T_1) and transverse (T_2) nuclear magnetic resonance (NMR) relaxation time constants can provide detailed insight into molecular dynamics [1]. In the case of fluids (gases and/or liquids) confined to porous materials, the acquisition of appropriate NMR relaxation data can further inform a variety of material and interfacial characteristics, including pore size distributions [2–4], pore network connectivity [5,6], adsorption interactions [7–9], and structural evolution rates [10,11]. Such observations have been expanded by the rock physics and petrochemical communities to fingerprint the presence of multiple fluids simultaneously. For example, in the case of hydrocarbon bearing shale formations, the presence of oil, gas, bitumen and clay-bound water may be inferred [12–14], while such analyses have also been employed in the field of heterogeneous catalysis to monitor competitive adsorption and displacement processes non-invasively [15,16].

In recent work we extended the interpretation of such phenomena to the identification of functional group resolved NMR relaxation [17]. Specifically, utilising a model mesoporous silica material imbibed with a wide range of polar protic liquid adsorbates, it was observed that the identification of multiple fluids within a single porous structure may be readily expanded

* Corresponding author. Department of Chemical Engineering, The University of Western Australia, 35 Stirling Highway, Perth, WA 6009, Australia.
E-mail address: neil.robinson@uwa.edu.au (N. Robinson).
Peer review under responsibility of Innovation Academy for Precision Measurement Science and Technology (APM), CAS.

https://doi.org/10.1016/j.mrl.2023.05.001

to the interpretation of a single fluid exhibiting multiple, distinct relaxation responses. In this paper we expand upon these observations, and apply T_1–T_2 relaxation correlation measurements to investigate the presence of functional group specific relaxation phenomena within the mesoporous metal oxide material gamma-alumina (γ-Al_2O_3) when saturated with 3-carbon polar-protic hydrocarbons (1-propanol, 2-propanol and propanoic acid).

2. NMR relaxation theory

The NMR relaxation time characteristics of fluids confined to porous materials are given by the well-known expressions [18]:

$$\frac{1}{T_1} \approx \frac{1}{T_1^{\text{bulk}}} + \rho_1 \frac{S}{V} \tag{1}$$

and

$$\frac{1}{T_2} \approx \frac{1}{T_2^{\text{bulk}}} + \rho_2 \frac{S}{V} + a t_e^{(k-1)}. \tag{2}$$

Here T_1 and T_2 are the measured longitudinal and transverse relaxation time constants of the system, while $T_{1,2}^{\text{bulk}}$ are the time constants for the unrestricted bulk fluid, where $T_1^{\text{bulk}} \approx T_2^{\text{bulk}}$. The term S/V represents the surface-to-volume ratio of the confining pore structure and $\rho_{1,2}$ are the surface relaxivities; such terms may be expanded as $\rho_{1,2} = \lambda / T_{1,2}^{\text{surf}}$ [19], where $T_{1,2}^{\text{surf}}$ are the relaxation time constants of an adsorbed surface layer thickness λ, and define enhanced rates of nuclear spin relaxation which occur at the solid-fluid interface through the modification of molecular dynamics upon adsorption [7], and through surface-adsorbate dipolar interactions with the pore surface [20,21]. Given $1/T_{1,2}^{\text{bulk}} \ll 1/T_{1,2}^{\text{surf}}$ (i.e. molecular dynamics are reduced within the adsorbed surface layer), the terms $1/T_{1,2}^{\text{bulk}}$ are often neglected.

For fluid-saturated mesoporous oxides, surface relaxation terms may be expanded as [20–22]:

$$\frac{1}{T_1^{\text{surf}}} \approx \beta [2J(\omega_0) + 8J(2\omega_0)] \tag{3}$$

and

$$\frac{1}{T_2^{\text{surf}}} \approx \frac{\beta}{2} [3J(0) + 5J(\omega_0) + 2J(2\omega_0)] \tag{4}$$

where

$$\beta \propto \sigma \delta^{-1} \gamma^4 \hbar^2 I(I+1). \tag{5}$$

Here σ is the surface spin density, δ is the distance of minimum approach between interacting dipolar pairs, and $\hbar$ is the reduced Planck constant; γ and I are the gyromagnetic ratio and nuclear spin quantum number of the spin system under study, respectively. The spectral density functions may be expressed as [20]:

$$J(\omega) = \tau_m \ln \left[\frac{1 + \omega^2 \tau_m^2}{(\tau_m/\tau_s)^2 + \omega^2 \tau_m^2} \right] \tag{6}$$

where $\omega = \{0, \omega_0, 2\omega_0\}$, wherein $\omega_0 = \gamma B_0$ is the Larmor frequency (in units of angular frequency) and B_0 is the applied field strength. Such expressions provide a direct relationship between measured relaxation phenomena and adsorbate dynamics, where the translational surface correlation time τ_m describes the average time taken for adsorbates to translate between adsorption sites at the pore surface, and the surface residence time τ_s describes the average time species spend within the adsorbed surface layer before desorption.

Finally, the last term in Equation (2) defines additional transverse relaxation phenomena resulting from magnetic susceptivity contrast $\Delta\chi$ between the porous solid and imbibed fluid (note that T_1 relaxation is insensitive to such phenomena), which result in the formation of effective internal magnetic field gradients of strength $g \sim \Delta\chi B_0$ [23–26]. Here a is a composite parameter which depends on the confining pore size l and adsorbate diffusivity D, and k defines any dependence on the experimental echo time t_e (defined in the Experimental Methods section below). For non-viscous fluids confined to small pores this term is characterised by $a \approx \gamma^2 \overline{g}^2 l^4 / (120D)$ and $k = 1$ (the motional averaged regime [27]), where $\overline{g}$ defines the average field gradient across the pore [26].

3. Experimental methods

3.1. Materials and sample preparation

Commercial mesoporous gamma-alumina (γ-Al_2O_3; mean pore size: 8 nm, specific surface area: 267 $m^2\,g^{-1}$) was obtained from Sasol in the form of 3 mm diameter spheres. Textural properties (pore size and surface area data) were obtained via nitrogen isotherm analysis at 77 K using a Micromeritics ASAP 2020 adsorption analyser. The material was activated under vacuum for 10 h at 200 °C to remove any physiosorbed water. The mean Barrett-Joyner-Halenda (BJH) pore size was obtained from the desorption branch of the isotherm, while the Brunauer-Emmett-Teller (BET) specific surface area was calculated from the adsorption branch within the relative pressure range 0.05–0.35.

For NMR analysis, the material was dried in air for 6 h at 110 °C. Cyclohexane (Thermofisher Scientific, >99%), 1-propanol (ChemSupply Australia, >99.8%), 2-propanol (ChemSupply Australia, >99.5%) and propanoic acid (ChemSupply Australia, >99%) were used as received. Imbibed porous γ-Al_2O_3 samples were prepared by soaking in excess liquid for at least 48 h under ambient conditions. The materials were then separated from each probe liquid and rolled over a pre-soaked filter paper to remove any excess liquid on the outer material surface, and transferred to sealed 7 mL glass vials and 5 mm NMR tubes for analysis.

3.2. NMR measurements

^{1}H nuclear spin relaxation measurements were performed across three spectrometers to provide data across a range of field strengths accessible by benchtop NMR hardware. Measurements were performed using (i) a $B_0 = 0.05$ T [$\omega_0(^1\mathrm{H})/(2\pi) = 2$ MHz] Magritek rock core analyser, (ii) a $B_0 = 0.3$ T [$\omega_0(^1\mathrm{H})/(2\pi) = 12.7$ MHz] Oxford Instruments Geospec spectrometer, and (iii) a $B_0 = 1$ T [$\omega_0(^1\mathrm{H})/(2\pi) = 43$ MHz] Magritek Spinsolve spectrometer. Default magnet temperatures (30 °C for measurements at 2 MHz and 12.7 MHZ, and 28 °C for measurements at 43 MHz) were employed in each case.

Two-dimensional (2D) T_1–T_2 relaxation correlation measurements were performed using the standard inversion recovery – CPMG (Carr-Purcell-Meiboom-Gill) sequence [28]. The direct (T_2) dimension of our 2D data was acquired by recording the magnitude of $n = 5000$ spin echoes separated by an echo time of $t_e = 250$ μs The indirect (T_1) dimension was encoded using $m = 32$ logarithmically spaced τ recovery times between 1 ms and 10 s, generating an ($m \times n$) data matrix. Measurements performed at 12.7 MHz and 43 MHz included four repeat scans, resulting in acquisition times of ~ 30 min and signal-to-noise ratios (SNR) of ~ 300 and ~ 1000, respectively. Measurements performed at 2 MHz included 16 repeat scans, resulting in acquisition times of ~ 2 h and SNR ~ 80. A recycle delay of 10 s ($\gg 5 \times T_1$) separated each repeat scan.

The resulting T_1–T_2 correlation data may be described by a 2D Fredholm integral equation of the first kind [29]:

$$\frac{S(nt_e,\tau)}{S(0,\infty)} = \iint K_{12}(T_2, nt_e, T_1, \tau) F(T_1, T_2)\, \mathrm{d}\log_{10}(T_1)\, \mathrm{d}\log_{10}(T_2) + \varepsilon(nt_e,\tau) \tag{7}$$

Here, $S(nt_e,\tau)/S(0,\infty)$ is the normalised spin echo magnitude and $\varepsilon(nt_e,\tau)$ is the experimental noise, which is assumed Gaussian with zero mean. The kernel function $K_{12}(T_2, nt_e, T_1, \tau)$ describes the expected form of T_1 and T_2 relaxation, and takes the form [29]:

$$K_{12}(T_2, nt_e, T_1, \tau) = \left[1 - 2\exp\left(\frac{-\tau}{T_1}\right)\right]\exp\left(\frac{-nt_e}{T_2}\right) \tag{8}$$

The desired distribution of T_1 and T_2 relaxation time constants $F(T_1, T_2)$ was obtained via an inverse Laplace transform of the acquired 2D relaxation data according to Equations (7) and (8). Stability was achieved through the application of Tikhonov Regularisation [30], with the degree of smoothing determined by the generalised cross-validation method [31]. Inversions were performed using an in-house fast Laplace inversion algorithm written in MATLAB (Mathworks Inc.), as first implemented by Mitchell et al. [32]. The resulting distributions were limited to (100 × 100) values with dimensions bound within the range $\{10^{-4}, 10^{1}\}$ s.

4. Results and discussion

To assess the expected relaxation response of fluids confined to our chosen porous material we first performed a 2D relaxation correlation measurement at 12.7 MHz using cyclohexane – a prototypical apolar and aprotic probe molecule with no labile ^{1}H environments. Fig. 1 shows the acquired correlation data for cyclohexane imbibed within γ-Al_2O_3, with a single correlation peak observed. Such data is characteristic of the imbibed probe fluid exhibiting a single effective ^{1}H relaxation environment as a result of rapid biphasic exchange between adsorbed species and bulk like molecules towards the centre of the pores, as described by Equations (1) and (2) [33,34]. The existence of a single correlation peak with narrow T_1 and T_2 distributions suggests that the pore network structure of the material assessed here is dominated by a single pore size (i.e., no hierarchical pore structure is expected [2]).

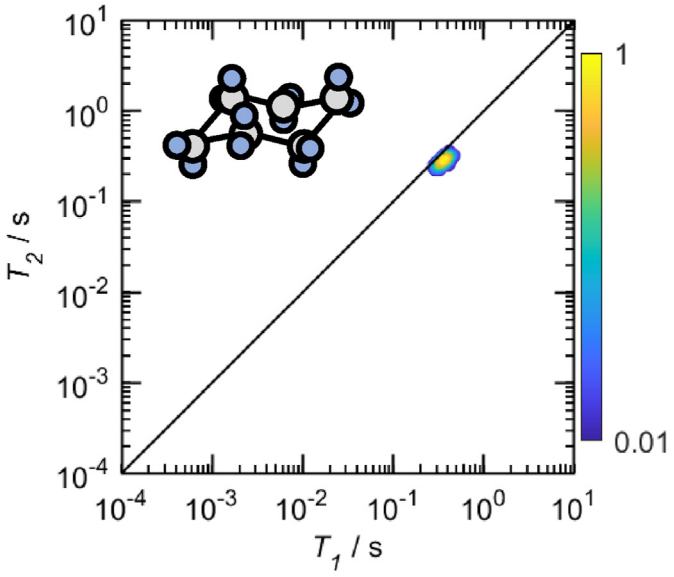

Fig. 1. ^{1}H T_1–T_2 correlation data for cyclohexane in mesoporous γ-Al_2O_3 at 12.7 MHz. The magnitude of the correlation peak indicates the relative probability of the system exhibiting a given combination of T_1 and T_2 relaxation time constants, as indicated by the colour bar. The solid diagonal line indicates the $T_1 = T_2$ parity ratio. The molecular structure of the cyclohexane adsorbate is also given: C and (aprotic) H atoms are coloured grey and blue, respectively.

Fig. 2 shows T_1–T_2 correlation data acquired for γ-Al_2O_3 imbibed with the three-carbon polar protic hydrocarbons 1-propanol, 2-propanol and propanoic acid, assessed across three field strengths between 2 MHz and 43 MHz. Three-carbon hydrocarbons are regularly employed as solvents and reagents within catalytic chemical processes involving mesoporous oxide materials [35–37], while the range of NMR spectrometer field strengths utilised here encompasses the typical array of permanent magnet-based benchtop NMR hardware applied to study fluids confined to porous systems [38–40]. Two distinct peaks are clearly apparent in each correlation plot, comprising a high intensity population at $T_2 \sim 10^{-2}$ s and low intensity population at $T_2 \sim 10^{-3}$ s in each case. Given that any interparticle liquid was removed during the preparation of these samples, together with the clear indication from our cyclohexane data in Fig. 1 that the porous material here does not exhibit significant pore size hierarchies, the existence of multiple correlation peaks within Fig. 2 cannot be ascribed to the relaxation characteristics of these probe molecules within pores of significantly different size and/or shape. Rather, such data is indicative of the existence of functional group specific relaxation phenomena, wherein multiple distinct relaxation times are observed for chemically distinct proton environments contained within the same probe molecule [17]. We assign the high intensity population within each data set to the aprotic alkyl ^{1}H-containing moiety of each adsorbate, while the lower intensity population is assigned to the protic hydroxyl moieties; these assignments are supported by our previous low-field investigation of alcohols and carboxylic acids imbibed within mesoporous silica [17], together with high-field spectrally resolved T_1 measurements of methanol within a separate γ-Al_2O_3 material [41], and fast field cycling investigations of similar systems [42]. As such, these data represent the first clear identification of 2D functional group resolved relaxation phenomena in mesoporous alumina for alcohol adsorbates larger than methanol, and the first such observation for a carboxylic acid within this material.

Enhanced rates of hydroxyl ^{1}H relaxation occur within porous oxides due to the coordination of such groups with solid surfaces upon adsorption, together with surface-adsorbed chemical exchange between adsorbing molecules and surface hydroxyl groups [17], which commonly terminate porous oxide materials (including aluminas [41,43]) at the pore surface. Observed relaxation characteristics then become a weighted average of such environments, with a clear reduction in hydroxyl group T_2, relative to that of the alkyl group, resulting from the very short transverse relaxation characteristics of solid-state protons. This behaviour is clear across the nine data sets shown in Fig. 2, exemplifying that such functional group specific relaxation phenomena may be observed for both a range of common hydrocarbon adsorbates (in this work a primary alcohol, secondary alcohol, and carboxylic acid) and a range of NMR field strengths. Clear differences are, however, apparent upon comparing the data acquired at 2 MHz to that acquired at increased field strengths, with significant correlation peak broadening observed at this low field strength. This observation is consistent with the low SNR of these data (SNR <100), and the corresponding broadening that is known to occur upon regularisation of low SNR relaxation data [44,45]. Notwithstanding such broadening effects, the multiple relaxation populations present within these systems are readily identifiable across the range of 2 MHz data, indicating that such hardware may provide an alternative to analysis at increased fields when considering porous material/adsorbate combinations which permit the acquisition of relaxation data at only very low fields; such measurements are of interest across a variety of materials ranging from iron rich geological samples [46] to paramagnet-

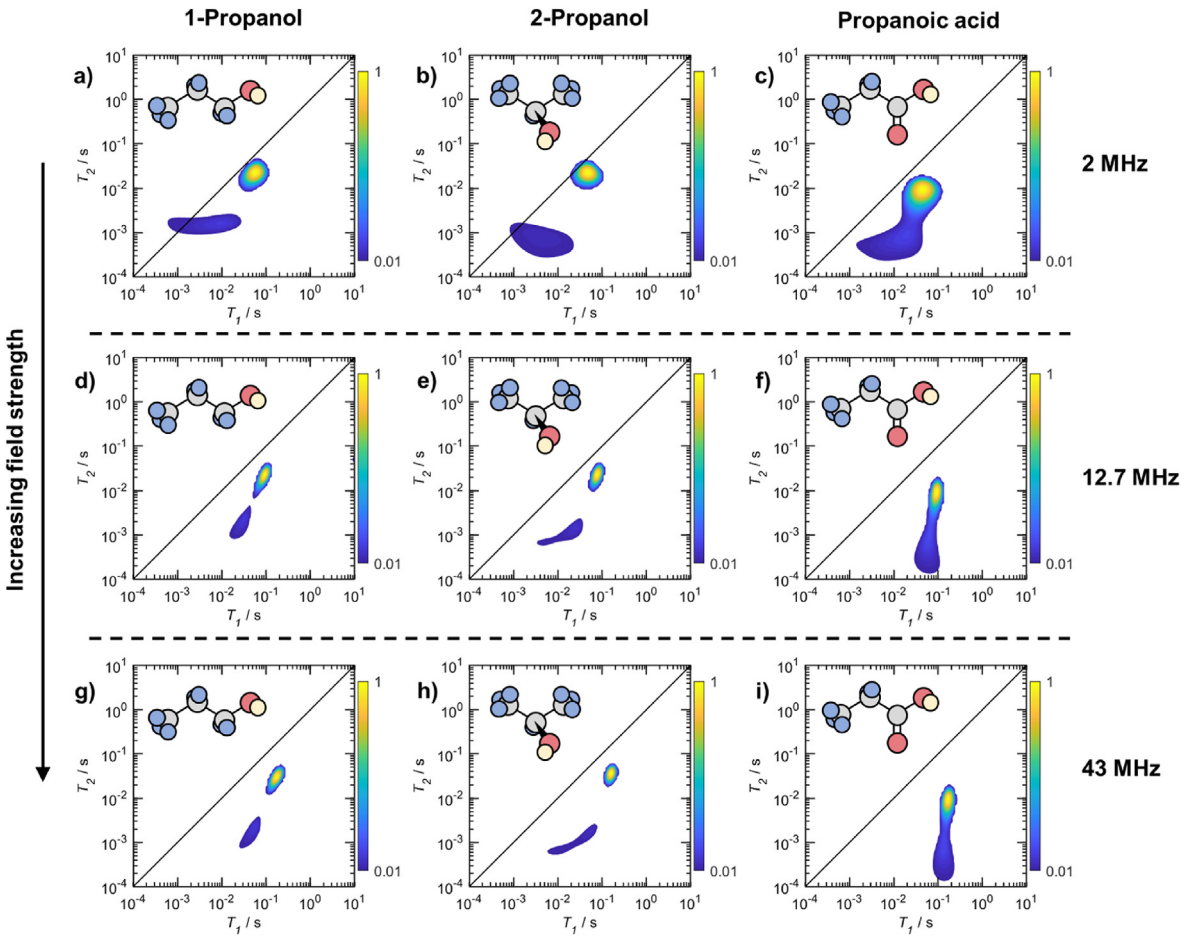

Fig. 2. ^{1}H T_1–T_2 correlation data for γ-Al_2O_3 imbibed with 1-propanol (left column; panels a), d) and g)), 2-propanol (centre column; panels b), e) and h)) and propanoic acid (right column; panels c), f) and i). Data is shown across three field strengths: top row data (panels a), b) and c)) were acquired at 2 MHz, middle row data (panels d), e) and f)) were acquired at 12.7 MHz, while bottom row data (panels g), h) and i)) were acquired at 43 MHz. The magnitude of each correlation peak indicates the relative probability of the system exhibiting a given combination of T_1 and T_2 relaxation time constants, as indicated by the colour bars. Solid diagonal lines indicate the $T_1 = T_2$ parity ratio. The molecular structure of each adsorbate is given: C and O are coloured grey and red, respectively. Aprotic H are coloured blue, while protic H are coloured yellow. Correlation peaks at long and short T_2 values are assigned to the relaxation behaviour of aprotic and protic ^{1}H-containing chemical moieties, respectively.

doped catalysts [47]. At the increased field strengths of 12.7 MHz and 43 MHz, narrow relaxation time distributions are evident, as expected following the inversion and regularisation of high SNR data [44,45].

Clear differences in the relative positioning of the alkyl and hydroxyl correlation peaks within Fig. 2 are also evident. Alcohol adsorbates present well separated correlation peaks, while there exists distinct population overlap in the case of propanoic acid; such overlap likely occurs here due to the small pore sizes (∼ 8 nm) of our γ-Al_2O_3 material, together with the high affinity of carboxylic acids for polar oxide surfaces [17], both of which drive the observed alkyl relaxation population to short T_2 values. Given this overlap, together with the observation that the T_2 relaxation characteristics of our hydroxyl populations lie close to the experimental echo time $t_e = 250$ μs employed in these measurements, we make no attempt here to quantify the relative populations of the two environments observed in Fig. 2, nor to interpret differences in the T_1/T_2 ratios of the correlation peaks.

Finally, a comparison of alkyl group relaxation characteristics across the range of NMR field strengths investigated allows us to briefly consider any influence of internal field gradients on these data. As described by Equation (2), T_2 relaxation processes with our γ-Al_2O_3 material may be perturbed in the presence of susceptibility contrast effects, the magnitude of which increase with applied field strength. Following Equations (1)–(6), an increase in observed T_1 and T_2 relaxation times is expected with increasing spectrometer field strength [24]. If internal field gradients dominate our measured T_2 data, however, a corresponding decrease in observed T_2 with increasing field strength will be observed [23]. Fig. 3 shows observed modal alkyl T_1 and T_2 relaxation time values (termed $\langle T_1 \rangle_{CH}$ and $\langle T_2 \rangle_{CH}$, respectively) as a function of field strength. An increase in $\langle T_1 \rangle_{CH}$ is observed, as expected, while the corresponding increase in $\langle T_2 \rangle_{CH}$ suggests that internal field gradient effects are negligible across the range of B_0 fields explored here.

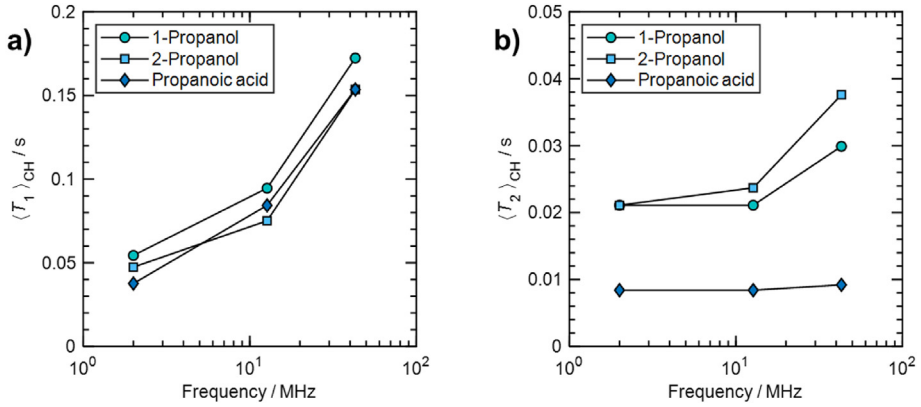

Fig. 3. Alkyl group ^{1}H T_1 (panel a)) and T_2 (panel b)) relaxation trends with NMR frequency for the three-carbon adsorbates 1-propanol, 2-propanol and propanoic acid imbibed within mesoporous γ-Al_2O_3. Data were acquired at 2 MHz, 12.7 MHz and 43 MHz.

5. Conclusion

In this work we have successfully demonstrated the existence of functional group resolved ^{1}H NMR relaxation phenomena within the mesoporous metal oxide material γ-Al_2O_3. These relaxation characteristics are observable for polar protic hydrocarbon adsorbates across NMR field strengths between 2 MHz and 43 MHz, encompassing typical field strengths exhibited by commercial low-field and benchtop NMR equipment. Such observations expand the range of materials known to exhibit such phenomena, and will aid in the application of NMR relaxation analysis to complex and heterogeneous porous systems by averting the inaccurate interpretation of relaxation data in terms of the existence of multiple adsorbates during displacement experiments, or when assessing the existence of multiple pore structures of different size. Overall, our results suggest measurements at $\geq$ 12.7 MHz provide suitable measurement conditions for the identification of such relaxation phenomena within metal oxides, facilitating the rapid acquisition high signal-to-noise ratio data at low-field.

CRediT authorship contribution statement

Neil Robinson: Conceptualization, Resources, Investigation, Formal analysis, Writing – original draft, Funding acquisition. **Carmine D'Agostino:** Conceptualization, Resources, Writing – review & editing. **Michael L. Johns:** Conceptualization, Writing – review & editing, Supervision, Funding acquisition.

Declaration of competing interest

The authors declare no conflicts of interest.

Acknowledgement

Neil Robinson gratefully acknowledges the support of the Forrest Research Foundation. Carmine D'Agostino would like to acknowledge the EPSRC for grant no. EP/S019138/1. The authors further acknowledge funding from The University of Western Australia through a Research Collaboration Award, and thank Sasol Ltd. for providing materials.

References

[1] J. Kowalewski, L. Mäler, Nuclear Spin Relaxation in Liquids: Theory, Experiments, and Applications, second ed., CRC Press, 2017.
[2] N. Robinson, R. Nasharuddin, G. Luo, A. Fourie, E.O. Fridjonsson, M.L. Johns, Pore structure evolution of cemented paste backfill observed with two-dimensional NMR relaxation correlation measurements, Ind. Eng. Chem. Res. 60 (2021) 13253–13264, https://doi.org/10.1021/ACS.IECR.1C01819.
[3] S. Davies, K.J. Packer, Pore-size distributions from nuclear magnetic resonance spin-lattice relaxation measurements of fluid-saturated porous solids. I. Theory and simulation, J. Appl. Phys. 67 (1998) 3163, https://doi.org/10.1063/1.345395.
[4] J.J. Chen, X. Kong, K. Sumida, M. Anne Manumpil, J.R. Long, J.A. Reimer, J.J. Chen, X. Kong, J.A. Reimer, K. Sumida, M.A. Manumpil, J.R. Long, Ex situ NMR relaxometry of metal–organic frameworks for rapid surface-area screening, Angew. Chem. Int. Ed. 52 (2013) 12043–12046, https://doi.org/10.1002/ANIE.201305247.
[5] M.A. Isaacs, C.M.A. Parlett, N. Robinson, L.J. Durndell, J.C. Manayil, S.K. Beaumont, S. Jiang, N.S. Hondow, A.C. Lamb, D. Jampaiah, M.L. Johns, K. Wilson, A.F. Lee, A spatially orthogonal hierarchically porous acid–base catalyst for cascade and antagonistic reactions, Nat Catal 3 (2020) 921–931, https://doi.org/10.1038/s41929-020-00526-5.
[6] N. Robinson, G. Xiao, P.R.J. Connolly, N.N.A. Ling, E.O. Fridjonsson, E.F. May, M.L. Johns, Low-field NMR relaxation-exchange measurements for the study of gas admission in microporous solids, Phys. Chem. Chem. Phys. 22 (2020) 13689–13697, https://doi.org/10.1039/d0cp02002h.
[7] N. Robinson, C. Robertson, L.F. Gladden, S.J. Jenkins, C. D'Agostino, Direct correlation between adsorption energetics and nuclear spin relaxation in a liquid-saturated catalyst, Material, ChemPhysChem. 19 (2018) 2472–2479, https://doi.org/10.1002/cphc.201800513.

[8] C. D'Agostino, J. Mitchell, M.D. Mantle, L.F. Gladden, Interpretation of NMR relaxation as a tool for characterising the adsorption strength of liquids inside porous materials, Chem. Eur J. 20 (2014) 13009–13015, https://doi.org/10.1002/chem.201403139.
[9] N. Robinson, P. Bräuer, A.P.E. York, C. D'Agostino, Nuclear spin relaxation as a probe of zeolite acidity: a combined NMR and TPD investigation of pyridine in HZSM-5, Phys. Chem. Chem. Phys. 23 (2021) 17752–17760, https://doi.org/10.1039/D1CP01515J.
[10] R. Nasharuddin, G. Luo, N. Robinson, A. Fourie, M.L. Johns, E.O. Fridjonsson, Understanding the microstructural evolution of hypersaline cemented paste backfill with low-field NMR relaxation, Cement Concr. Res. 147 (2021), 106516, https://doi.org/10.1016/J.CEMCONRES.2021.106516.
[11] N. Robinson, R. Nasharuddin, E.O. Fridjonsson, M.L. Johns, NMR surface relaxivity in a time-dependent porous system, Phys. Rev. Lett. 130 (2023), 126204, https://doi.org/10.1103/PhysRevLett.130.126204.
[12] M. Fleury, M. Romero-Sarmiento, Characterization of shales using T1-T2 NMR maps, J. Pet. Sci. Eng. 137 (2016) 55–62, https://doi.org/10.1016/j.petrol.2015.11.006.
[13] Y.-Q. Song, R. Kausik, NMR application in unconventional shale reservoirs – a new porous media research frontier, Prog. Nucl. Magn. Reson. Spectrosc. 112–113 (2019) 17–33, https://doi.org/10.1016/J.PNMRS.2019.03.002.
[14] K. Yang, P.R.J. Conolly, L. Liu, X. Yang, N. Robinson, M. Li, M. Mahmoud, A. El-Husseiny, M. Verrall, E.F. May, M.L. Johns, Quantitative characterization of methane adsorption in shale using low-field NMR, J. Nat. Gas Sci. Eng. 108 (2022), 104847, https://doi.org/10.1016/j.jngse.2022.104847.
[15] D. Weber, J. Mitchell, J. Mcgregor, L.F. Gladden, Comparing strengths of surface interactions for reactants and solvents in porous catalysts using Two-dimensional NMR relaxation correlations, J. Phys. Chem. C 113 (2009) 6610–6615, https://doi.org/10.1021/jp811246j.
[16] M. Leutzsch, A.J. Sederman, L.F. Gladden, M.D. Mantle, In situ reaction monitoring in heterogeneous catalysts by a benchtop NMR spectrometer, Magn. Reson. Imaging 56 (2019) 138–143, https://doi.org/10.1016/j.mri.2018.09.006.
[17] N. Robinson, E.F. May, M.L. Johns, Low-field functional group resolved nuclear spin relaxation in mesoporous silica, ACS Appl. Mater. Interfaces 13 (2021) 54476–54485, https://doi.org/10.1021/ACSAMI.1C13934.
[18] Y.Q. Song, Magnetic resonance of porous media (MRPM): a perspective, J. Magn. Reson. 229 (2013) 12–24, https://doi.org/10.1016/j.jmr.2012.11.010.
[19] Y.Q. Song, H. Cho, T. Hopper, A.E. Pomerantz, P.Z. Sun, Magnetic resonance in porous media: recent progress, J. Chem. Phys. 128 (2008), 052212, https://doi.org/10.1063/1.2833581.
[20] S. Godefroy, J.-P. Korb, M. Fleury, R.G. Bryant, Surface nuclear magnetic relaxation and dynamics of water and oil in macroporous media, Phys. Rev. E 64 (2001), 021605, https://doi.org/10.1103/PhysRevE.64.021605.
[21] J. Mitchell, L.M. Broche, T.C. Chandrasekera, D.J. Lurie, L.F. Gladden, Exploring surface interactions in catalysts using low-field nuclear magnetic resonance, J. Phys. Chem. C 117 (2013) 17699–17706, https://doi.org/10.1021/jp405987m.
[22] P.J. McDonald, J.-P. Korb, J. Mitchell, L. Monteilhet, Surface relaxation and chemical exchange in hydrating cement pastes: a two-dimensional NMR relaxation study, Phys. Rev. E 72 (2005), 011409, https://doi.org/10.1103/PhysRevE.72.011409.
[23] J. Mitchell, T.C. Chandrasekera, L.F. Gladden, Obtaining true transverse relaxation time distributions in high-field NMR measurements of saturated porous media: removing the influence of internal gradients, J. Chem. Phys. 132 (2010), 244705, https://doi.org/10.1063/1.3446805.
[24] J. Mitchell, T.C. Chandrasekera, M.L. Johns, L.F. Gladden, E.J. Fordham, Nuclear magnetic resonance relaxation and diffusion in the presence of internal gradients: the effect of magnetic field strength, Phys. Rev. E 81 (2010), 026101, https://doi.org/10.1103/PhysRevE.81.026101.
[25] J. Mitchell, T.C. Chandrasekera, L.F. Gladden, Measurement of the true transverse nuclear magnetic resonance relaxation in the presence of field gradients, J. Chem. Phys. 139 (2013), 074205, https://doi.org/10.1063/1.4818806.
[26] J. Mitchell, T.C. Chandrasekera, Understanding generalized inversions of nuclear magnetic resonance transverse relaxation time in porous media, J. Chem. Phys. 141 (2014), 224201, https://doi.org/10.1063/1.4903311.
[27] M.D. Hürlimann, K.G. Helmer, T.M. Deswiet, P.N. Sen, C.H. Sotak, Spin echoes in a constant gradient and in the presence of simple restriction, J. Magn. Reson. 113 (1995) 260–264, https://doi.org/10.1006/JMRA.1995.1091.
[28] Y.-Q. Song, L. Venkataramanan, M.D. Hürlimann, M. Flaum, P. Frulla, C. Straley, T1–T2 correlation spectra obtained using a fast two-dimensional Laplace inversion, J. Magn. Reson. 154 (2002) 261–268, https://doi.org/10.1006/JMRE.2001.2474.
[29] L. Venkataramanan, , Yi-Qiao Song, M.D. Hurlimann, Solving Fredholm integrals of the first kind with tensor product structure in 2 and 2.5 dimensions, IEEE Trans. Signal Process. 50 (2002) 1017–1026, https://doi.org/10.1109/78.995059.
[30] A.N. Tikhonov, V.I.A. Arsenin, Solutions of Ill-Posed Problems, SIAM, 1977.
[31] G.H. Golub, M. Heath, G. Wahba, Generalized cross-validation as a method for choosing a good ridge parameter, Technometrics 21 (1979) 215–223, https://doi.org/10.1080/00401706.1979.10489751.
[32] J. Mitchell, D.A. Graf von der Schulenburg, D.J. Holland, E.J. Fordham, M.L. Johns, L.F. Gladden, Determining NMR flow propagator moments in porous rocks without the influence of relaxation, J. Magn. Reson. 193 (2008) 218–225, https://doi.org/10.1016/j.jmr.2008.05.001.
[33] K.R. Brownstein, C.E. Tarr, Importance of classical diffusion in NMR studies of water in biological cells, Phys. Rev. A (Coll Park). 19 (1979) 2446–2453, https://doi.org/10.1103/PhysRevA.19.2446.
[34] P.J. Barrie, Characterization of porous media using NMR methods, Annu. Rep. NMR Spectrosc. 41 (2000) 265–316, https://doi.org/10.1016/s0066-4103(00)41011-2.
[35] M. Tamura, Y. Nakagawa, K. Tomishige, Recent developments of heterogeneous catalysts for hydrogenation of carboxylic acids to their corresponding alcohols, Asian J. Org. Chem. 9 (2020) 126–143, https://doi.org/10.1002/AJOC.201900667.
[36] C. Sievers, S.L. Scott, Y. Noda, L. Qi, E.M. Albuquerque, R.M. Rioux, Phenomena affecting catalytic reactions at solid–Liquid interfaces, ACS Catal. 6 (2016) 8286–8307, https://doi.org/10.1021/ACSCATAL.6B02532.
[37] S. Najafishirtari, K. Friedel Ortega, M. Douthwaite, S. Pattisson, G.J. Hutchings, C.J. Bondue, K. Tschulik, D. Waffel, B. Peng, M. Deitermann, G.W. Busser, M. Muhler, M. Behrens, A perspective on heterogeneous catalysts for the selective oxidation of alcohols, Chem. Eur J. 27 (2021) 16809–16833, https://doi.org/10.1002/CHEM.202102868.
[38] J. Mitchell, E.J. Fordham, Contributed Review: nuclear magnetic resonance core analysis at 0.3 T, Rev. Sci. Instrum. 85 (2014), 111502, https://doi.org/10.1063/1.4902093.
[39] J. Mitchell, L.F. Gladden, T.C. Chandrasekera, E.J. Fordham, Low-field permanent magnets for industrial process and quality control, Prog. Nucl. Magn. Reson. Spectrosc. 76 (2014) 1–60, https://doi.org/10.1016/J.PNMRS.2013.09.001.
[40] B. Blümich, K. Singh, Desktop NMR and its applications from materials science to organic Chemistry, Angew. Chem. Int. Ed. 57 (2018) 6996–7010, https://doi.org/10.1002/anie.201707084.
[41] N. Robinson, L.F. Gladden, C. D'Agostino, Exploring catalyst passivation with NMR relaxation, Faraday Discuss 204 (2017) 439–452, https://doi.org/10.1039/C7FD00098G.
[42] J. Ward-Williams, J.-P. Korb, L. Rozing, A.J. Sederman, M.D. Mantle, L.F. Gladden, Characterizing solid–liquid interactions in a mesoporous catalyst support using variable-temperature fast field cycling NMR, J. Phys. Chem. C 125 (2021) 8767–8778, https://doi.org/10.1021/acs.jpcc.1c00218.
[43] M. Digne, P. Sautet, P. Raybaud, P. Euzen, H. Toulhoat, Hydroxyl groups on γ-alumina surfaces: a dft study, J. Catal. 211 (2002) 1–5, https://doi.org/10.1006/jcat.2002.3741.
[44] D. Bernin, D. Topgaard, NMR diffusion and relaxation correlation methods: new insights in heterogeneous materials, Curr. Opin. Colloid Interface Sci. 18 (2013) 166–172, https://doi.org/10.1016/j.cocis.2013.03.007.
[45] J. Mitchell, T.C. Chandrasekera, L.F. Gladden, Numerical estimation of relaxation and diffusion distributions in two dimensions, Prog. Nucl. Magn. Reson. Spectrosc. 62 (2012) 34–50, https://doi.org/10.1016/J.PNMRS.2011.07.002.
[46] K.T. O'Neill, D. Langford, E.O. Fridjonsson, M.L. Johns, Quantitative analysis of diffusion regimes in iron ore with low field NMR, Geophys. J. Int. 232 (2022) 2017–2034, https://doi.org/10.1093/gji/ggac421.
[47] C. D'Agostino, P. Bräuer, Exploiting enhanced paramagnetic NMR relaxation for monitoring catalyst preparation using $T_1 - T_2$ NMR correlation maps, React. Chem. Eng. 4 (2019) 268–272, https://doi.org/10.1039/C8RE00173A.

Neil Robinson completed an MChem Chemistry degree at Cardiff University, followed by a PhD in Chemical Engineering at the University of Cambridge. He currently holds a Forrest Research Foundation Fellowship at The University of Western Australia, and is a Strategic Research Fellow within the Future Energy Exports Cooperative Research Centre. His research focuses on the development and characterisation of next-generation materials for energy, environmental and societal applications, with a strong focus on understanding gas and liquid dynamics within functional porous media using magnetic resonance.